

Fermilab
ES & H Section

R. P. Note No. 120

DETERMINATION OF THE SECONDARY ELECTRON EQUILIBRIUM USING AN
EXTRAPOLATION CHAMBER

January 1996

Written By: Jane S. P. [Signature] Date: 1/2/96

Written By: Don [Signature] Date: 1/4/96

Written By: [Signature] Date: 1-4-96

Written By: [Signature] Date: 1/2/96

Reviewed By: [Signature] Date: 1/10/96

Approved By: [Signature] Date: 1/10/96

Distribution:

RP Staff, RPTS Staff

DETERMINATION OF THE SECONDARY ELECTRON EQUILIBRIUM USING AN EXTRAPOLATION CHAMBER

RADIATION PHYSICS NOTE 120

E. Marshall, D. Cossairt, F. Krueger, K. Vaziri

January 1996

INTRODUCTION

To ensure that the external personnel dosimetry program conducted by U.S. Department of Energy contractors is of the highest quality, the DOE established the Department of Energy Laboratory Accreditation Program or DOELAP (DOE 1986a,b). The contractor's dosimetry program is assessed against the criteria set forth for dosimeter performance and the associated quality assurance and calibration programs (DOE 1986a). During the onsite assessment conducted of Fermilab's external dosimetry program during May 1994, an observation with regard to equipment maintenance and calibration was made: "calibration personnel should probably review the electron secondary equilibrium needs at various irradiation distances from the Cs-137 irradiation systems." (Dolecek & Mei 1994)

The majority of the secondary electrons are generated through interactions of the beam with the collimator. Secondary electrons increase the low energy component of the radiation field, increasing the shallow doses measured. For dosimetric purposes, this increase needs to be defined so appropriate corrections to calculations or modifications to the facility can be made. Prompted by this observation, a study was designed to investigate the electron secondary equilibrium by determining the dose equivalent as a function of depth in a tissue-equivalent medium in the facility used for blind testing of the personnel dosimeters used on-site. This paper summarizes the methodology utilized and the results of the investigation.

EXPERIMENTAL APPARATUS

The Radiation Physics Calibration Facility consists of three shielded caves, a mezzanine area for low-scatter neutron irradiations, a storage area, and workshop. For the most part, all gamma irradiations for the purposes of calibration of radiation protection instrumentation and badge spiking are performed in one of the caves. This cave, the Source Projector Facility (Krueger & Larson 1993), is constructed of concrete and consists of an outer control room and an inner irradiation room. Two J.L. Shepard, Inc. projectors are operated from the outer room. One of the projectors (Model 28-10) contains a nominal 100 Ci Cs-137 source. The other is a dual projector (Model 78-1M) containing two sources with nominal activities of 10 Ci and 1 Ci Cs-137. The sources are raised from the safe storage position by rods and are returned by gravity. A collimator has been installed to allow use of a standard brass rod mounted source. An electronic timer interfaced to the projectors provides for accurate timing of irradiations.

The source projectors and collimator are mounted on an elevated rolling stand in the outer room, with their radiation cones directed into the irradiation room through a port. The beam is collimated such that it has a divergence of 30° for the largest Cs-137 source (~100 Ci) and 20° for the other sources. The desired projector is rolled into position on the stand to align with the port for irradiation into the inner room. An instrument/detector positioning carriage is roller-mounted to floor rails along the beam axis inside the inner room. The detector carriage distance from the source may be adjusted remotely from the outer room using a hand crank. The height of the carriage is readily adjustable by means of a crank-operated elevating mechanism.

For the depth-dose measurements, an extrapolation chamber (EG&G Model EIC-1) was used (EGG 1974). The electrode spacing is variable, between 0.25 mm and 4.3 mm, and is adjusted by rotating an aluminum ring which holds the entrance window. There is a reference mark on the ring to allow measurements to be replicated. In this experiment, approximate plate separations of 1.3 mm, 2.3 mm, 3.3 mm and 4.3 mm were used in the collection of data.

The instrument was mounted on a stand and aligned with the center of the beam and at a distance of 1 m from the source. Disks of tissue equivalent plastic were placed in front of the chamber and the current was measured at various thicknesses to develop the depth-dose curves presented later in this report. The ion chamber window, constructed of conductive polyethylene, has a nominal density thickness of 2.9 mg/cm², which was added to that of the disks to determine the total density thickness.

The currents generated within the extrapolation chamber are quite small, on the order of 0.1 pA, even using the largest source. A Keithley Model 610 Electrometer was used to measure the charge and its output fed into a Keithley Model 617 Electrometer (Krueger 1995), used in the voltmeter mode for its data storage capabilities. Since a relatively high leakage was measured with the Keithley 617 Electrometer, it was not used for charge collection directly.

Data were collected using the Keithley 617's race-track data collection capability. The source was raised and the instrumentation was permitted to stabilize in the radiation field. The Keithley 617 Electrometer was placed into data storage mode and the integrated voltage recorded at 10 second intervals. Although the 617 contains an internal timer, known inaccuracy in this timer prompted the use of an external timer. A full scale measurement on the Keithley 610 Electrometer resulted in a 3 V output as measured by the Keithley 617. By correcting for leakage and the scale setting of the Keithley 610 Electrometer, the net collected charge was calculated.

Figure 1 shows a schematic drawing of the equipment setup.

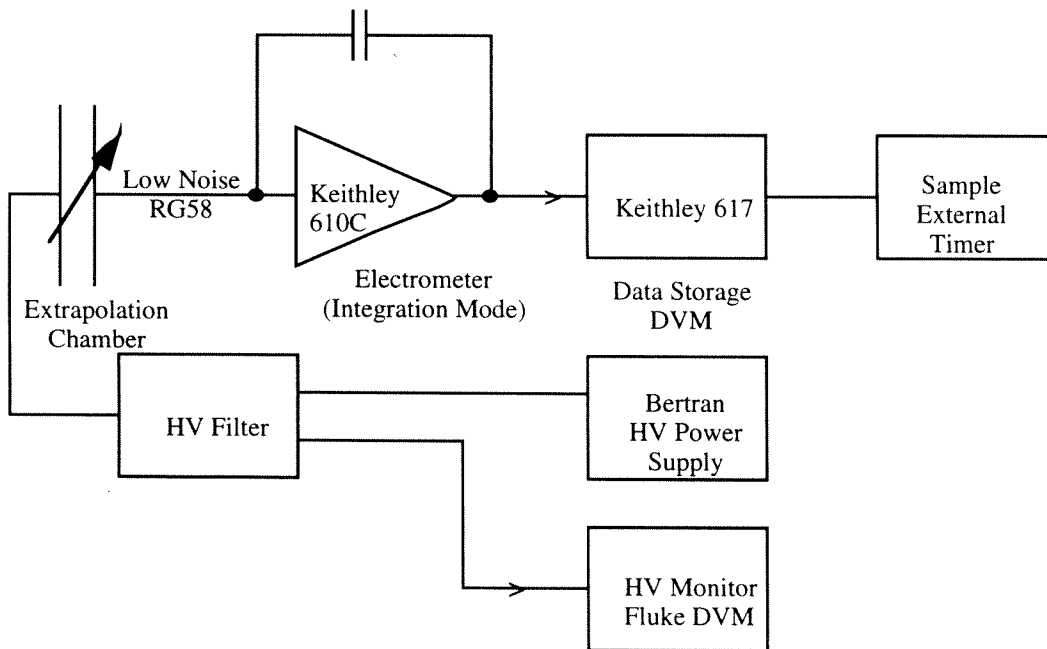


Figure 1: Schematic of Experimental Apparatus

MEASUREMENTS AND RESULTS

Plate Separation Measurements

The extrapolation chamber specification sheet listed nominal values for the plate separation at each turn of the chamber: 0.3 mm at 0 turn and then 1 mm per turn. The instrument data sheet accompanying the chamber listed the minimum plate separation (or plate spacing at 0 turns) at 0.25 mm. However, no accurate values for the plate separation at each turn of the plate was specified. Measurements were taken using calipers to determine the actual plate separations. Due to the chamber's small size, the overall length of the chamber at each turn was measured and not the actual distance of the plate separation. Assuming the separation at 0 turns is 0.25 mm and that the difference in the chamber length is equal to the distance moved by the plate during one turn, the plate separations were calculated. These values (Table 1) for the plate separation were used in determining the effective area of the plate and subsequent calculation of the exposure rate.

Table 1: Extrapolation Chamber Measured Plate Separations

Turn Number	Plate Separation (mm)
0	0.25
1	1.25
2	2.23
3	3.20
4	4.30

Effective Area of Plate

Fringe fields and other physical phenomena affect the effective area of any capacitor. To account for these, the effective area rather than the actual plate area should be used in subsequent calculations of the dose equivalent.

The capacitance of the chamber was measured to determine the effective area of the capacitor at each plate separation. At a given plate separation, the collected charge was measured directly with the Keithley 610 at four different applied biases (-25V, -50V, -75V, and -100V). Applying the equations for calculating the capacitance, the effective area could be calculated.

$$(1) \quad A = \frac{Cd}{k\epsilon_0} = \frac{qd}{Vk\epsilon_0}$$

- where A=effective area (m²)
- C = capacitance
- d=plate separation (m)
- k=dielectric constant of air at 1 atm = 1.00059
- ε₀ = permittivity of vacuum = 8.854187817E-12 C²/J · m
- q=collected charge (C)
- V=applied bias (V)

The measured values were averaged to derive the effective area for the given plate separation. Table 2 presents these results. These should be compared to the nominal value reported in the extrapolation chamber specifications of 0.785 cm².

Table 2: Effective Area at Various Plate Separations

Plate Separation (mm)	Area (cm ²)	Standard Deviation of Area (cm ²)
1.25	0.815	0.006
2.23	0.790	0.003
3.20	0.781	0.003
4.30	0.802	0.014

The effective areas calculated were factored into the calculation of absorbed dose rate from the measured values of integrated current.

Determination of Operating Voltage Gradient

During the operation of the extrapolation chamber, it is desirable to maintain a constant voltage gradient over all the measurements at various plate separations. A measurement was made of the collected charge versus the applied voltage with the chamber set at one turn. The apparatus was placed at 1 meter from the largest Cs-137 source (137-8.1-1), exposing it to a field of approximately 21 R/hr. Figure 2 plots the values obtained and indicates when saturation is reached.

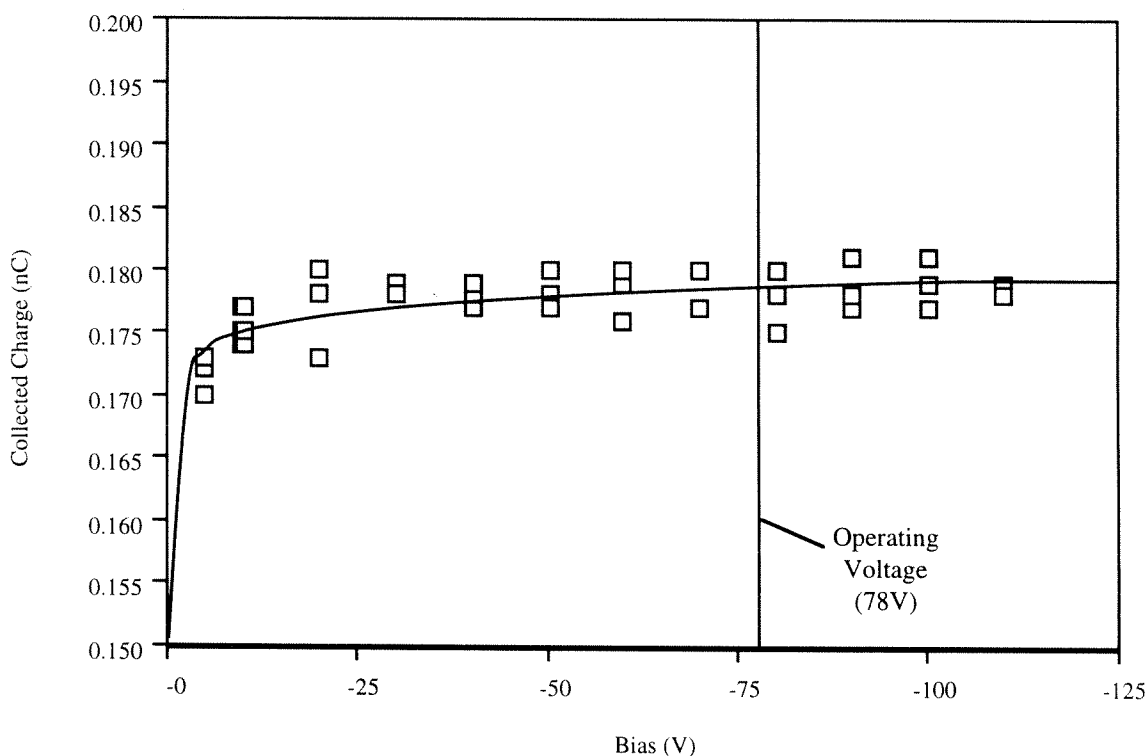


Figure 2: Operating Voltage Gradient Determination

After reviewing the data in Figure 2, a voltage gradient of approximately -60 V/mm was chosen. This choice was based on criteria of being well away from the knee region of the curve and below the manufacturer's specification of -100 V/mm maximum. This gradient was then used to determine the operating voltage for each of the other plate separations.

Depth-Dose Measurements

Figures 3 - 6 plot the measured current at each density thickness of absorber for the various plate separations. These graphs also show two regression curve fits. Note that the scale of the ordinates differ from graph to graph. The first curve fit is based on an approach presented by M.J. Scannell (1995). This curve fit is of the form:

$$(2) \quad y = a + bx + \frac{c}{x}$$

where a, b, and c are arbitrary fit parameters. The second fit employs a model which includes an initial dose buildup followed by an exponential falloff and is of the form:

$$(3) \quad y = a(1 - e^{-bx})(e^{-cx})$$

again, where a, b and c are fit parameters. In general, the second curve (Equation 3) provides a better fit to the data, as demonstrated by the square of the correlation coefficient. However, given the errors in the measurements and the lack of data between 2.9 mg/cm² and 41.4 mg/cm², both equations provide an adequate empirical fit to these data. The lack of data between 2.9 mg/cm² and 41.4 mg/cm² was due to the lack of absorbers of uniform density thickness in this range.

The goal of this investigation was to determine the shallow to deep dose ratio. Shallow dose is the absorbed dose at a tissue depth equal to 7 mg/cm² and deep dose is the absorbed dose at a tissue depth equal to 1000 mg/cm² (DOE 1986b). Equations 2 and 3 as fitted to the integrated current data for each separation were used to obtain values for the current at a depth of 7 mg/cm² and at a depth of 1000 mg/cm² (Table 3). These calculated values of current at 7 mg/cm² and 1000 mg/cm² were graphed against plate separation as shown in Figures 7 and 8. Given the physical constraint that at 0 mm plate spacing, there is zero current, each of the four plots (7 mg/cm² or 1000 mg/cm² for Equation 2 or Equation 3) can be fit with a linear curve of the form y=mx. The ratio of the slopes for the 7 mg/cm² and 1000 mg/cm² curves yields the shallow to deep dose ratios given in Table 4.

Table 3: Current at Shallow and Deep Dose Depths

Equation 2 Fit			Equation 3 Fit		
Turns	Current @ 7 mg/cm ² (pA)	Current @ 1000 mg/cm ² (pA)	Turns	Current @ 7 mg/cm ² (pA)	Current @ 1000 mg/cm ² (pA)
1	0.1876	0.1792	1	0.1897	0.1792
2	0.3454	0.3290	2	0.3486	0.3291
3	0.5008	0.4906	3	0.5062	0.4906
4	0.6569	0.6392	4	0.6599	0.6391

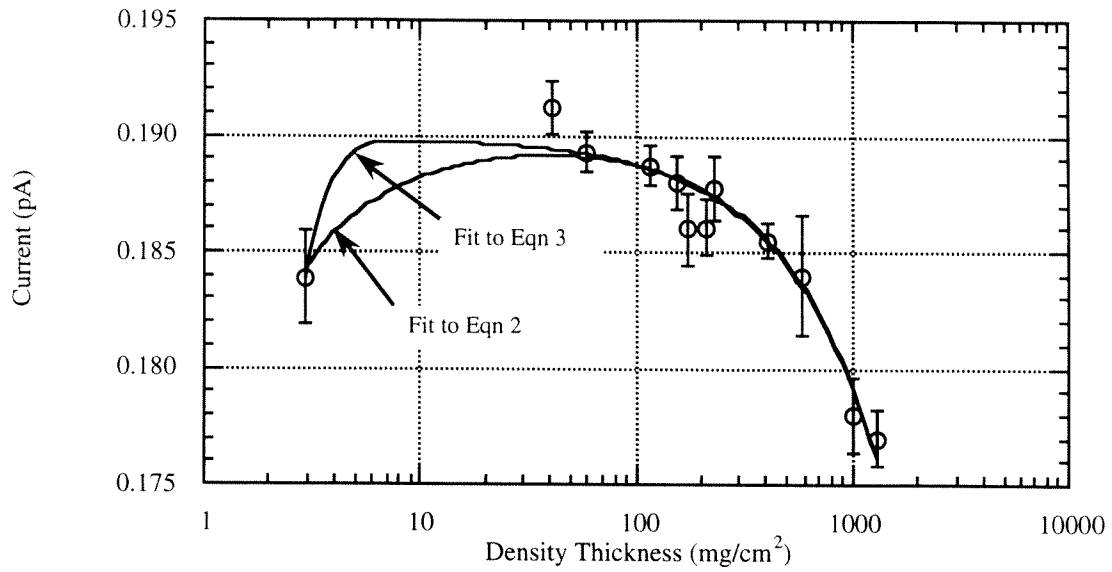


Figure 3: Density Thickness Versus Current at 1 Turn

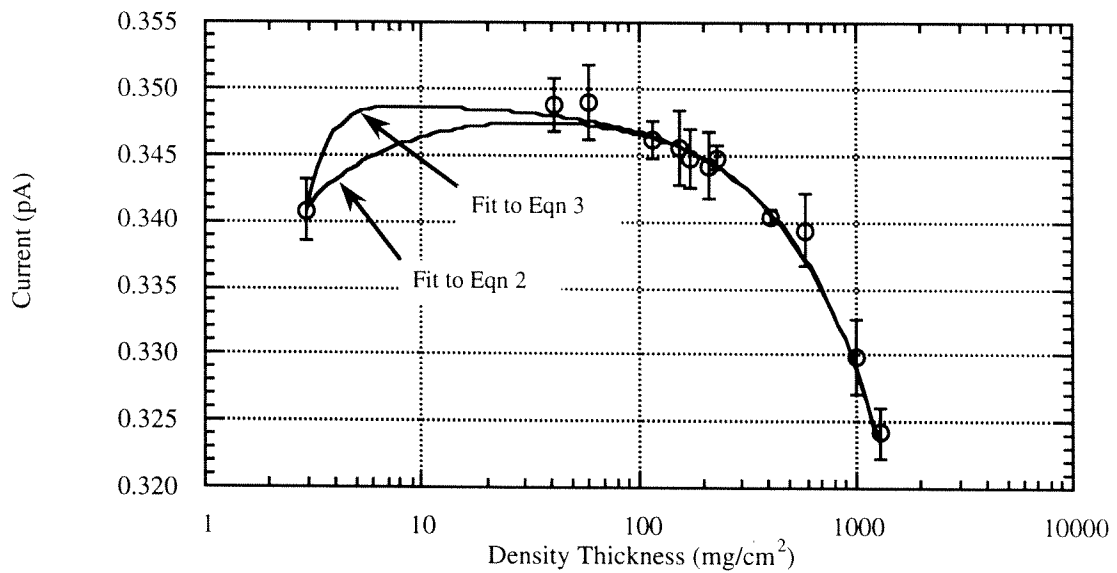


Figure 4: Density Thickness Versus Current at 2 Turns

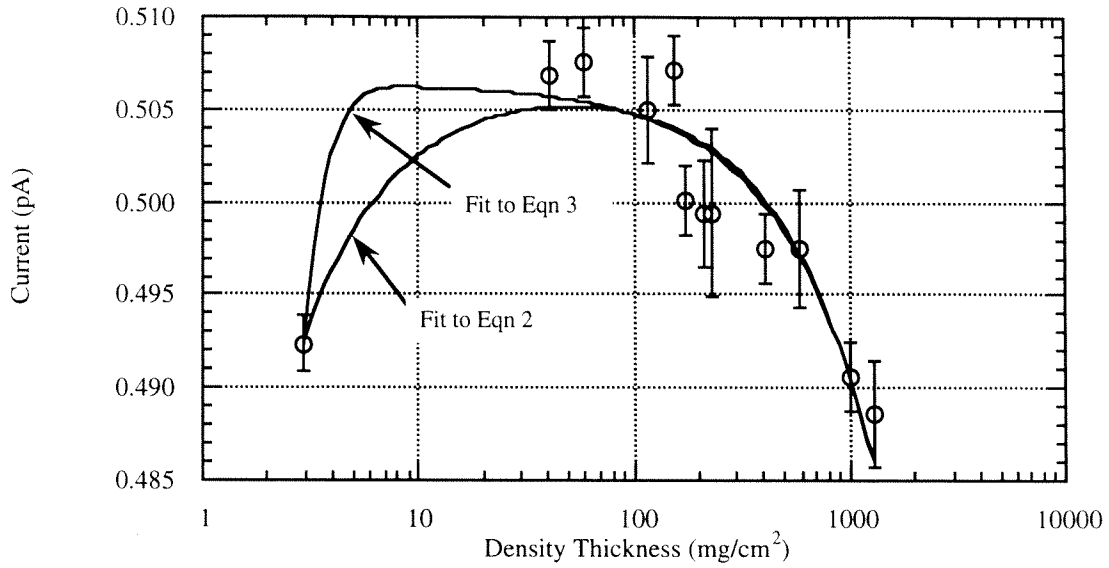


Figure 5: Density Thickness Versus Current at 3 Turns

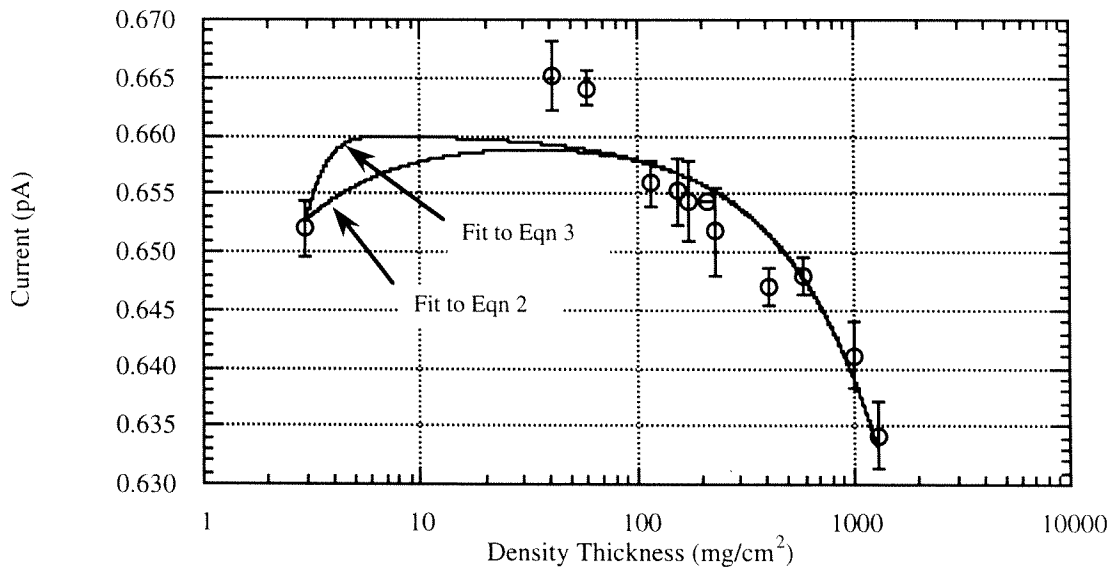


Figure 6: Density Thickness Versus Current at 4 Turns

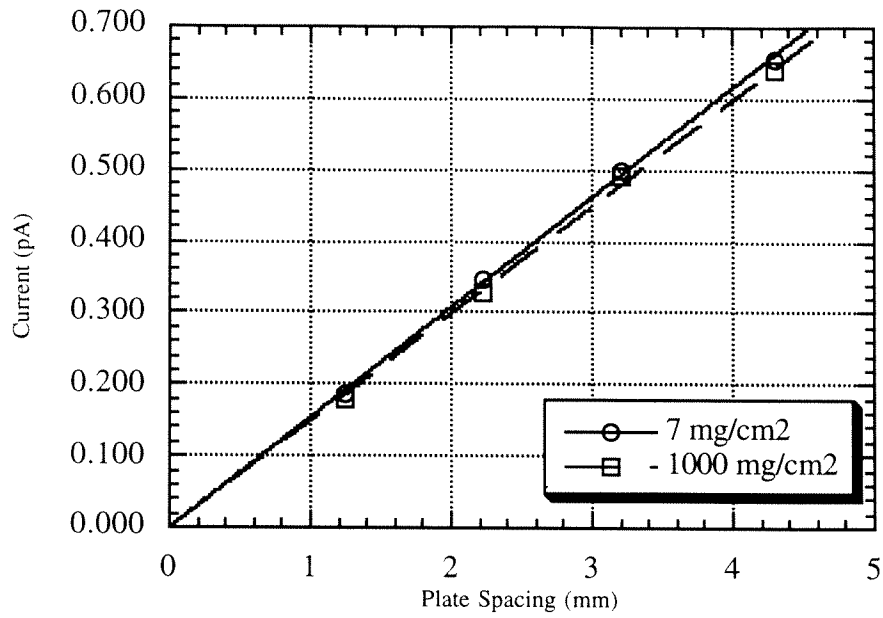


Figure 7: Determination of Shallow to Deep Dose Ratio (Equation 2)

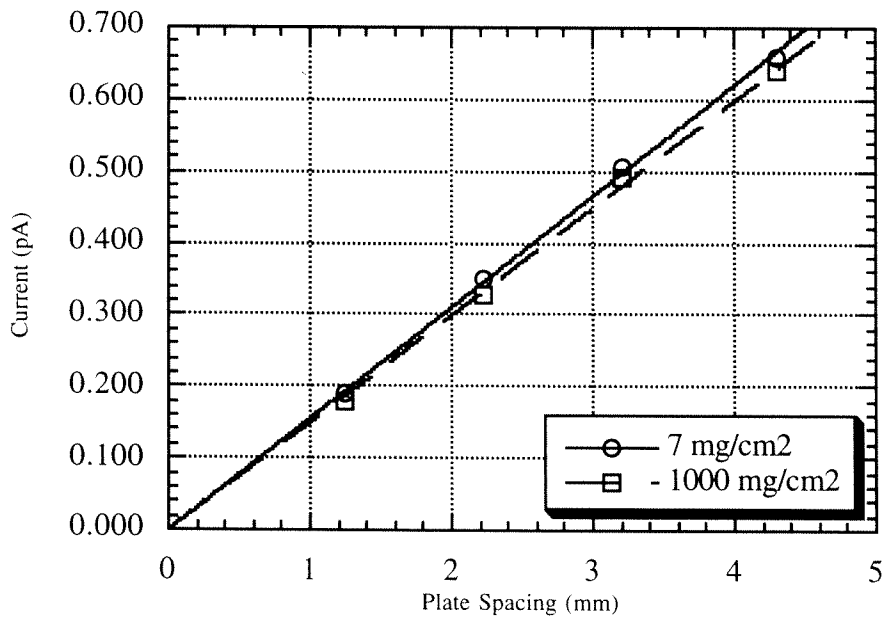


Figure 8: Determination of Shallow to Deep Dose Ratio (Equation 3)

Table 4: Extrapolation Results

Equation Number	Slope @ 7 mg/cm ²	Slope @ 1000 mg/cm ²	Ratio
2	0.1540	0.1496	1.029
3	0.1552	0.1496	1.037

Estimation of Absorber Thickness

Although Cs-137 emits two betas, 0.514 MeV (93.5%) and 1.176 MeV (6.5%), the majority of the shallow dose seen by the detector is due to secondary electrons produced by Compton scattering off the collimator and source holder. The betas originating from the radioactive decay of the source are ranged out by the source holder, with some production of bremsstrahlung. The secondary electrons can be mathematically described as being similar to a beta radiation source with a continuous spectrum. It has been experimentally observed that the transmission curve for beta radiation emitted from a source is best fit by an exponential curve (Knoll 1979):

$$(4) \quad \frac{I}{I_0} = e^{-nt}$$

where n = absorption coefficient
 t = absorber thickness
 I = count rate (or comparable) with absorber
 I_0 = count rate (or comparable) without absorber

Tsoufanides (1983) provides a formula to estimate the absorption coefficient.

$$(5) \quad n \left(\frac{m^2}{kg} \right) = 1.7(E_{max})^{-1.14}$$

where E_{max} = maximum energy of the beta particle (MeV)

The maximum energy of a secondary electron is given by the Compton edge. Thus, the maximum energy of a secondary electron is very close to the gamma ray energy emitted from the Cs-137 source, 0.6616 MeV. Solving Equation 5, n is equal to 2.72 m²/kg or 27.23 cm²/g.

Because the transmission is described by an exponential, eliminating all of the secondary electrons is impractical. It is possible to reduce the number of secondary electrons such that their contribution to the shallow dose is negligible. This can be achieved by arbitrarily assuming a ratio for I/I_0 of 0.001 or 0.1%. With this ratio and the value of n calculated previously, the absorber thickness that would achieve this ratio is estimated to be 0.254 g/cm² (2.76 mm polyethylene).

An alternative way to estimate the absorber thickness is to use an empirical formula to determine the range of the particles (Shleien 1992):

$$(6) \quad R = 0.412E^{1.265-0.0954 \ln E}$$

OR

$$(7) \quad R = 0.542E - 0.133 \text{ [Feather's Rule]}$$

Using these equations, the absorber thickness is estimated to be 0.240 g/cm² or 0.226 g/cm², respectively. These are comparable to the value determined using Equation 4.

Any amount of shielding would also be expected to attenuate the deep dose. Through interpolation, the mass attenuation coefficient for a Cs-137 gamma ray in polyethylene is found to be 0.0885 cm²/g (Shielen 1992). By introducing an additional 0.254 g/cm² of polyethylene into the beam, the gamma absorbed dose rate and hence, the deep dose rate, would be expected to decrease by approximately 2%.

These calculations are only estimates. If any absorber material is introduced into the beam to eliminate the secondary electrons, additional measurements will need to be performed to verify the effect of the absorber material on the shallow to deep dose ratio and the overall dose rate.

Calculation of Conversion Factor Between Integrated Current and Absorbed Dose Rate

For comparison purposes, the absorbed dose rate was calculated from this data. Measurements have already been performed using NIST traceable instrumentation and sources to determine the exposure rate of the Cs-137 source used in this experiment. Calculation of the absorbed dose rate is dependent upon a number of factors: the effective area, the plate separation, the density of air, the ionization potential, the relative mass stopping power of tissue to air and the current generated by the chamber. These factors are related by the Bragg-Gray principle:

$$(8) \quad D\left(\frac{\text{Gy}}{\text{s}}\right) = \frac{S * W\left(\frac{\text{J}}{\text{C}}\right)}{\rho\left(\frac{\text{kg}}{\text{mm}^3}\right) * A(\text{mm}^2) * d(\text{mm})} * \frac{Q(\text{C})}{t(\text{s})}$$

where D = dose rate
 S = relative mass stopping power
 W = ionization potential
 ρ = density of air at NTP (22°C and 1 atm)
 A = effective area of the chamber plate
 d = plate separation
 Q = charge collected by the chamber
 t = integration time

The charge collected was corrected for temperature and pressure differences by employing the ideal gas law. The correction for humidity was negligible.

For a given plate separation, $\frac{S * W}{\rho * A * d}$ is a constant. NCRP Publication 112 provides an appropriate value for S equal to 1.13 (NCRP 1991). W was taken to be 35 J/C based on information in Knoll (1979) Using the values previously determined for A and d, this constant for each plate separation is equal to the values presented in Table 5.

Table 5: Determination of Conversion Factor From Current to Absorbed Dose Rate

Turn Number	Conversion Factor (Gy/C)
1	3.223E+08
2	1.863E+08
3	1.314E+08
4	9.513E+07

A Microsoft Excel™ spreadsheet was used to record the data, correct for the background and leakage, and normalize to NTP. Using the measurements at 2.9 mg/cm², the absorbed dose rate at each of the various turns can be derived (Table 6).

Table 6: Dose Rates at Various Plate Spacings

Plate Spacing (mm)	Current (pA)	Absorbed Dose Rate (rad/hr)
1.25	0.1839 ± 0.0020	21.342 ± 0.231
2.23	0.3408 ± 0.0024	22.863 ± 0.159
3.20	0.4924 ± 0.0015	23.290 ± 0.073
4.30	0.6520 ± 0.0025	22.329 ± 0.084

A linear extrapolation to 0 mm plate spacing results in an absorbed dose rate of 21.579 rad/hr. For comparison, the source strength as measured using the NIST traceable instrumentation and then correcting for decay was 21.041 R/hr or 19.989 rad/hr using the tissue conversion factor of 0.95 rad/R.

The dose rate obtained using the extrapolation chamber and that measured by NIST traceable instruments are about 8% different. This can partially be explained by the fact that the NIST traceable instruments have walls that are sufficiently thick enough to shield out all of the betas and low energy x-rays. The instrument wall thickness also serves to decrease the overall dose rate by attenuating the gammas as well. Another explanation may lie within the values chosen for W and S in calculating the dose conversion factors. The range of values for W are from 33.85 J/C to 35 J/C depending upon the reference; the range of values for S are from 1.13 to 1.15. In the calculations reported here, the extremes were chosen for both W and S. This may account for approximately 3% and about 2% of the discrepancy, respectively. The center of the detector was not marked. It was assumed that the center of the detector was the same as the center of the chamber. The extrapolation chamber essentially results in measurement at a point, by design, because of the extremely small detector volume. The NIST traceable instrumentation has a finite size relative to the source. There are many other factors that may be contributing to the higher dose rate measured by the extrapolation chamber. To fully understand the discrepancy, additional studies will need to be conducted. For the purposes of this paper, the discrepancy is not of crucial importance.

DISCUSSION/CONCLUSIONS

For calibration purposes, it is desirable to have the ratio of the shallow to deep dose equal to 1.00 (Murphy et al. 1991). Taking the ratio of the calculated values, it is seen that the shallow dose in the Source Projector Facility is higher than the deep dose (1.029-1.037 depending on the fit used), indicating that additional material to attenuate the beam is necessary. This analysis quantifies the effect of secondary electrons on the dose rate and allows appropriate corrections to be made in the calibration of instruments and quality assurance checks of the dosimetry vendor. An estimate has been made of the absorber thickness required to attenuate the secondary electrons. Should the approximately 3 mm of polyethylene be introduced into the Source Projector Facility, additional measurements would be required to verify the effectiveness of the absorber and its affect on the overall dose rate.

REFERENCES

- DOE 1986a U. S. Department of Energy. Handbook for the Department of Energy Laboratory Accreditation Program for Personnel Dosimetry Systems. Washington, DC: U.S. DOE; DOE/EH-0026. 1986.
- DOE 1986b U. S. Department of Energy. Department of Energy Standard for the Performance Testing of Personnel Dosimetry Systems. Washington, DC: U.S. DOE; DOE/EH-0027; 1986.
- Dolecek & Mei 1994 Department of Energy Laboratory Accreditation Program Site Assessment Report for the Fermi Dosimetry Program. E.H. Dolecek and G. T. Mei. May, 18, 1994.
- EGG 1974 EG&G, Inc. Extrapolation Ion Chamber -- Model EIC-1 Data Sheet 84. April 1974.
- Knoll 1979 Knoll, G.F. Radiation Detection and Measurement. New York: John Wiley and Sons, 1979.
- Krueger & Larson 1993 Krueger, F. and J. Larson. Fermilab ES&H Section Source Projector Facility Operating Procedures. April 1993.
- Krueger 1995 Krueger, F. Operation of Instrumentation Used for Gamma Ray source Transfer Calibration and Facility Studies. R.P. Note 111. March 1995.
- Murphy et al. 1991 Murphy, M.K., R.J. Traub, J.C. McDonald, and C.D. Hooker. Physical Characterization of a Cs-137 Field Used for Proficiency-Test Irradiations. Health Physics. 60:789-796.
- NCRP 1991 NCRP Report Number 112. Calibration of Survey Instruments Used in Radiation Protection for the Assessment of Ionizing Radiation Fields and Radioactive Surface Contamination. Bethesda, MD: National Council on Radiation Protection and Measurements, December 31, 1991.
- Tsoufanidis 1983 Tsoufanidis, N. Measurement and Detection of Radiation. New York: Hemisphere Publishing Corporation, 1983.
- Scannell 1995 Scannell, M.J. Extrapolation Chamber Techniques For Measuring Absorbed Dose Rate, PEP Lecture at HPS Annual Meeting, July 1995.
- Shleien 1992 Health Physics and Radiological Health Handbook. Edited by B. Shleien. Silver Spring, MD: Scinta, Inc., 1992.